Densification Effects on Critical-Current Dependence on Longitudinal Strain in $Bi_2Sr_2CaCu_2O_{8+x}$ Wires

Najib Cheggour, Emsley L. Marks, Jianyi Jiang, *Senior Member, IEEE*, Ernesto Bosque, and David C. Larbalestier, *Fellow, IEEE*

***Abstract*—There is undoubted new interest in applying $Bi_2Sr_2CaCu_2O_{8+x}$ (Bi-2212) superconducting round wires for ultra-high fields above 20 T. We investigated effects of filament densification in a high-quality Bi-2212 wire made with fine Engi-Mat powder by comparing critical-current I_c dependence on longitudinal strain ε among samples reacted under 5- and 50-bar overpressure during the partial-melt process. The Walters spring apparatus we used for transport $I_c(\varepsilon)$ measurements had a high sensitivity that helps detect the first onset of irreversible damage, as well as determine other characteristic strains that describe the transition of $I_c(\varepsilon)$ from weak to steeper dependences. Results show a noticeable improvement of all the tensile characteristic strains as a result of densification. For example, average value of the irreversible strain limit ε_{irr} increased from 0.3% for 5-bar samples to 0.4% for 50-bar specimens. Moreover, the response of densified samples to strain was significantly more homogeneous along the sample length, independent of the measurement mode used. These improvements, which happened in conjunction with an increase of I_c by a factor 2.5 at 16 T and 4.2 K, are plausibly due to the elimination of pores that can concentrate stress in strained, nondensified samples where they act as crack initiators. Sensitivity of densified samples to longitudinal compression, on the other hand, increased for strain values beyond −0.28%. In this case, we believe that the continuum of Bi-2212 material in densified samples facilitates the propagation of strain-induced buckling defects as compared to nondensified samples where pores may slow this propagation and keep damage more localized. The benefits of densification, nevertheless, largely outweigh this increase of sensitivity at high compression as I_c remained significantly higher than that of nondensified samples. These results reveal very positive effects of filament densification on the conductor's strain properties that add to the significant boost of I_c it induces.**

***Index Terms*—Bi-2212, densification, irreversible strain limit, porosity, strain properties.**

Received 30 August 2024; revised 31 January 2025 and 23 March 2025; accepted 2 April 2025. Date of publication 9 April 2025; date of current version 2 May 2025. This work was supported in part by the U.S. Department of Energy, Office of Science, Office of High Energy Physics under Grant DE-SC0017657 and Grant DE-SC0010421, in part by the National High Magnetic Field Laboratory (NHMFL) supported by the National Science Foundation Cooperative Agreements under Grant DMR-1644779 and Grant DMR-2128556, and in part by the State of Florida. *(Corresponding author: Najib Cheggour.)*

Najib Cheggour, Jianyi Jiang, Ernesto Bosque, and David C. Larbalestier are with the Applied Superconductivity Center, National High Magnetic Field Laboratory, Florida State University, Tallahassee, FL 32310 USA (e-mail: ncheggour@asc.magnet.fsu.edu).

Emsley L. Marks is with Magnet Science & Technology, National High Magnetic Field Laboratory, Florida State University, Tallahassee, FL 32310 USA.

Color versions of one or more figures in this article are available at https://doi.org/10.1109/TASC.2025.3559406.

Digital Object Identifier 10.1109/TASC.2025.3559406

I. Introduction

TRANSPORT critical-current density J_c of superconducting $Bi_2Sr_2CaCu_2O_{8+x}$ multifilamentary round wires (referred to as Bi-2212) has reached values in excess of 6600 and 4600 A/mm^2 at 15 and 30 T, respectively, at 4.2 K and 1 μV/cm electric-field criterion E_c [1]. These high J_c values are enabled by the use of partial-melt heat treatments on wires under overpressure (OP-HT) that highly densifies the Bi-2212 filaments and thus eliminates pores impeding the flow of supercurrent through the conductor, by understanding how to optimize solidification from the melt so as to generate a good biaxial texture, and by the advent of new techniques for producing Bi-2212 powder [1], [2], [3], [4], [5], [6], [7], [8], [9], [10]. These advances have renewed interest in Bi-2212 for fabricating laboratory magnets, particle-accelerator dipoles, nuclear magnetic resonance systems, and various other devices to target field intensities in the range of 20 T and beyond [11], [12], [13], [14], [15], [16], [17], [18], [19], [20], [21].

In the ultra-high magnetic-field environment, the resilience of the conductor to the Lorentz force and the mitigation of the hoop and transverse stresses resulting from this force are among the driving questions for further research to qualify Bi-2212 magnet technology. The matrix of a typical Bi-2212 wire is made of pure Ag with an Ag-Mg reinforcing outer sheath. After undergoing a partial-melt heat-treatment at elevated temperatures close to 900 °C, the conductor usually has a tensile yield strength ($\sigma_{0.2}$) and a Young's modulus in the range of 130 MPa and 70 GPa, respectively, with a highly nonlinear stress-strain characteristic [22], [23]. To preclude detrimental effects on magnet performance from these modest mechanical characteristics and to avoid cracking of the brittle Bi-2212 filaments, mechanical reinforcements at both the conductor and the magnet levels are being investigated, supported by detailed simulations of strain in magnet operating conditions [20], [21], [23], [24], [25], [26], [27], [28], [29], [30]. Reinforcement aspects are undoubtedly essential for the success of this technology. They require input on the conductor's limits of strain and stress that initiate Bi-2212 cracking and need a good understanding of its failure modes.

Even though strain properties of Bi-2212 conductors have been studied and models proposed in the past [31], [32], [33], [34], [35], [36], [37], [38], [39], [40], [41], some ambiguities in the current understanding of these properties remain. Moreover, historically, most of the strain investigations made were on nondensified Bi-2212 wires that are no longer considered viable

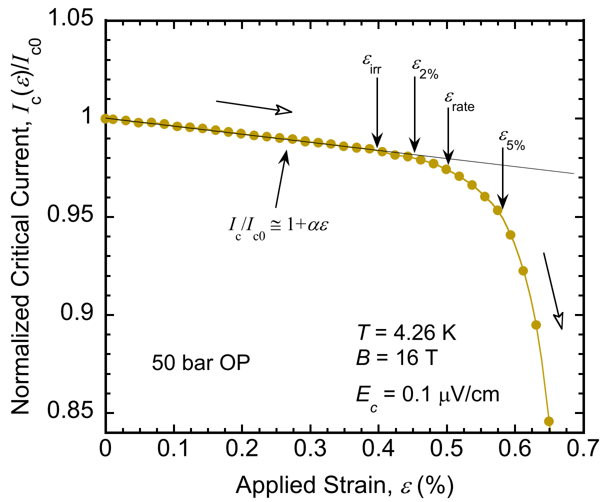

Fig. 1. Representative dataset of I_c/I_{c0} dependence on longitudinal tensile strain ε, obtained on a densified Bi-2212 sample at 16 T, 4.26 K, and 0.1 μV/cm. Characteristic strains ε_{irr}, $\varepsilon_{2\%}$, ε_{rate}, and $\varepsilon_{5\%}$ are marked by arrows. The graph shows a typical spread of the so-called "strain limit" from 0.4% to 0.6 % depending solely on how it is defined in literature.

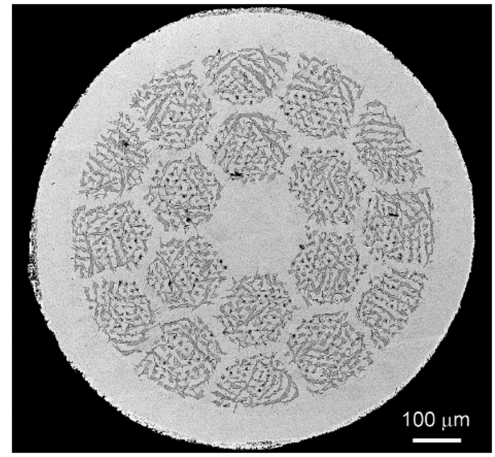

Fig. 2. Transverse cross-section of Bi-2212 85 × 18 multifilamentary wire PMM180410 after 50-bar OP-HT. The wire diameter decreased to 0.97 mm from 1.0 mm due to filament densification.

for magnet applications. The current know-how indeed makes OP-HT an indispensable procedure. Given that OP-HT densifies the microstructure of Bi-2212 filaments considerably, it could possibly alter the strain properties and failure modes in densified conductors. So far, reports on densified Bi-2212 wires have been scarce and rather inconclusive on whether their resilience to strain improves with densification.

Godeke et al. [35] reported a value for the so-called "strain limit" of densified Bi-2212 wires of about 0.3% at 4.2 K—the strain limit being broadly considered as the strain value not to exceed in fabricating and operating magnets to avoid failure. For densified samples that had some handling damage prior to measurements, this strain limit was in the range of 0.4%–0.5% [35]. Bjoerstad et al. [37] reported on measurements made at 77 K on densified samples that were slightly underdoped after OP-HT to maximize I_c at this temperature. They showed a strain limit of 0.6% where, after strain unloading, I_c degraded by 5% with respect to its initial value at that same unloaded strain [37]. The authors anticipated a slightly higher strain limit at 4.2 K if the matrix' mechanical properties improved from those at 77 K. Other authors reported values of the strain limit of about 0.4% for densified samples [39], [40]. Strain-limit values for nondensified Bi-2212 samples were about 0.3% and 0.5% [31], [41], also scattered like those for densified samples. These studies used different Bi-2212 wires and, hence, it is difficult to draw definitive conclusions on densification effects.

In fact, and before attempting data comparisons, it is important to note that the definition of the so-called "strain limit" is not necessarily the same in literature. There are no standard procedures yet in place for doing strain measurements on Bi-2212 conductors and for analyzing data to extract the "strain limit". Cheggour and Marks [42] addressed this topic in a separate paper, the essence of which is summarized in Fig. 1 where different characteristic strains are indicated on an $I_c(\varepsilon)$ curve obtained for a densified Bi-2212 specimen. Clearly, the different strain-limit definitions are far from being equivalent. The irreversible strain limit ε_{irr} is the strain that initiates irreversible behavior of $I_c(\varepsilon)$, presumably indicating the onset of crack formation in Bi-2212 material. Strains $\varepsilon_{2\%}$ and $\varepsilon_{5\%}$ correspond to where I_c degradation reaches 2% and 5% of the virgin value I_{c0} (prior to sample straining), respectively. Finally, ε_{rate} is where the first change of $I_c(\varepsilon)$ degradation rate occurs. This strain was introduced in [42] following analysis of detailed $I_c(\varepsilon)$ datasets. The exact meaning and relevance of ε_{rate} is currently unclear. It might correspond to the first observable spreading of damage after its initiation at ε_{irr}.

From Fig. 1, it is evident that different strain-limit definitions lead to quite different results. Due to the gradual degradation of $I_c(\varepsilon)$ for $\varepsilon_{irr} < \varepsilon < \varepsilon_{5\%}$, it is not yet clear which of these strains is most important for designing and operating magnets. It is probably useful for magnet designers to know all of them for a given Bi-2212 conductor because they characterize the transition of $I_c(\varepsilon)$ from weak to steeper dependences. In this article, we will systematically provide these characteristic strains. We will use them to directly compare densified and nondensified samples of the same Bi-2212 billet in order to explore the still open question concerning the effect of densification on Bi-2212 strain properties.

II. Experimental

A. Conductor Investigated and OP-HT Cycles

The Bi-2212 multifilamentary round wire studied herein had 1530 filaments separated by pure Ag matrix and distributed among 18 bundles (85 × 18 design). The bundles were restacked in Ag-0.2wt%Mg outer sheath. The conductor was manufactured by Bruker-OST by use of the powder-in-tube technique. The Bi-2212 precursor powder was fabricated by Engi-Mat by use of the nanospray combustion chemical vapor condensation method. The starting billet (number PMM180410) was 10 kg in weight and yielded a single wire length of 1.4 km at a final diameter of 1.0 mm. The wire was not twisted. Fig. 2 shows a transverse cross-section of a wire sample that received an OP-HT at 50 bar.

Each of the samples investigated was wound on an Inconel-600 mandrel for OP-HT. Sample length was 2.2 m approximately and its ends were sealed to enable full densification and to prevent leakage of material during heat treatment. Profiles of OP-HT had multiple stages at various dwelling temperatures, times, and ramp rates, such as in [1] for example. We used 5- and 50-bar overpressure values in separate OP-HT cycles. The 5-bar cycle was used to obtain nondensified samples. The small 5 bar overpressure was to counter internal pressure of gases in the wire during the partial-melt process in order to prevent leakage of material through the wire matrix. This cycle was performed at a maximum temperature of 888 °C. Time in the melt, defined as the interval between the times temperature reached 884 °C and 872 °C during sample heat-up and cool-down, respectively [43], was 3.7 h approximately. The 50-bar OP-HT cycle was to obtain highly densified samples. It was performed at a maximum temperature of 889 °C. Time in the melt was 2.2 h approximately. The slight differences in the 5- and 50-bar OP-HT profiles (other than the overpressure value) should not influence data comparisons and conclusions made in this report. Samples had no visible leakages after heat treatment.

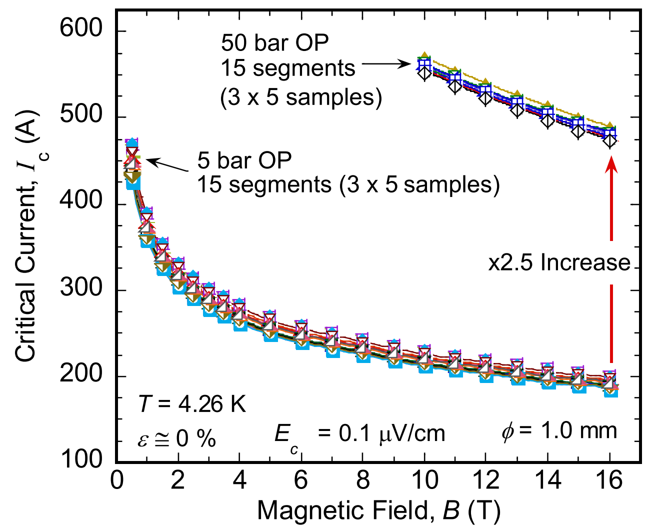

Fig. 3. Results of $I_c(B)$ at zero applied strain, 4.26 K, and 0.1 μV/cm, for five densified (50-bar OP) and five nondensified (5-bar OP) Bi-2212 wire samples. Measurements were taken on three segments (8 cm long each) per sample. I_c was homogeneous and increased for the densified samples by a factor 2.50 at 16 T.

B. Strain Device and Measurement Modes

The device used to apply longitudinal strain to the sample is a Walters spring made of Cu-2%Be alloy [44], [45], [46]. It has a wide elastic-strain range from –1% to +1%. We provided ample details in [42] on the procedure for transferring a sample from the reaction mandrel onto the spring and for soldering the two together. We reiterate that Cu-Be material is particularly suitable for making strain devices on which a Bi-2212 sample is soldered (such as a Walters spring, a U-bending spring [35], [40], or a Pacman [47]). As reported by Sugano et al. [41] thermal contraction of Cu-Be from room temperature to 5 K matches that of a typical Bi-2212 composite wire extremely well, such that a Bi-2212 conductor sample soldered to a Cu-Be beam should experience practically no prestrain upon cooling to liquid He temperature.

Soldering of the sample onto the spring was done at ≈ 200 °C by use of Pb37%–Sn63% eutectic solder. Multiple pairs of voltage taps were attached to the sample. The principal ones were three pairs (taps 1, 2, and 3) attached to the sample section that is on the spring turns, each pair monitoring one sample turn (or segment) ≈ 8 cm in length. This allows us to evaluate homogeneity over a 24 cm length of each sample.

The apparatus was inserted into a superconducting magnet cryostat. Measurements of the sample current versus voltage (*I-V*) were made in liquid He at 4.26 K and in magnetic field up to 16 T. The latter was perpendicular to the current and oriented such that the Lorentz force applied to the sample was directed inward. Values of I_c were determined from *I-V* curves at E_c of 0.1 μV/cm. Expanded uncertainties due to random effects in estimating I_c and $\varepsilon_{\mathrm{irr}}$ (and the other characteristic strains) were 2% and 0.04% strain, respectively.

We measured *I-V* curves at 16 T as a function of ε either in tension or in compression. We used the following three measurement modes.

1) *Monotonic-loading mode (I)*: Strain was monotonically increased each time by a constant and small amount close to 0.02%. For measurements in compression, strain increment was about -0.02%.
2) *Load/partial-unload mode (II)*: Strain was monotonically increased by 0.02% until it reached $\varepsilon \approx 0.18\%$. Strain was then partially unloaded by a constant step $\Delta\varepsilon$. Measurements were conducted in both the loaded and partially unloaded states to check reversibility of I_c versus ε. This was repeated multiple times while incrementally increasing ε. The strain step $\Delta\varepsilon$ was either –0.11% or –0.15 % for different samples.
3) *Load/full-unload mode (III)*: Unlike in the load/partial-unload mode, strain was brought back to 0% after each loaded strain value. Hence, the unloading step $\Delta\varepsilon$ increased with ε.

We measured 10 samples in total, five 50-bar and five 5-bar samples. For each sample, we measured three turns (or segments). We followed the same data-analysis methods described in [42] to compare densified and nondensified samples in each of these modes.

Nomenclature of samples measured in tension is "mode"-"sample number." For example, sample I-1 was sample 1 measured in mode I (in tension). Samples measured in compression (all in mode I) are labeled I-c "sample number" (for example, sample I-c1).

III. Results

A. Magnetic-Field Effect at Zero Applied Strain

Prior to applying strain, we conducted I_c measurements as a function of ascending magnetic field up to 16 T. Results obtained on the 50- and 5-bar samples (i.e., 15 segments of each group), at 4.26 K and 0.1 μV/cm, are depicted in Fig. 3. Variation of I_c

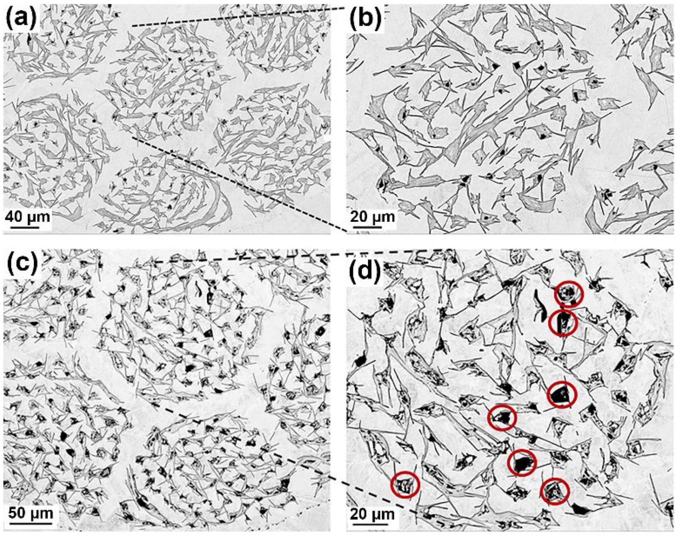

Fig. 4. SEM images from cross-sections of Bi-2212 conductors showing microstructural details of (a) three of the inner and outer filament bundles after 50-bar OP-HT, (b) one inner filament bundle shown in (a), (c) three of the inner and outer filament bundles after 5-bar OP-HT, (d) one inner filament bundle shown in (c). Filaments were free from pores in (a)–(b) confirming high densification of the 50-bar sample. In contrast, (c) and (d) show the presence of large pores within Bi-2212 filaments in the 5-bar sample, highlighted by red circles in (d).

among all segments was 0.9% for the 50-bar samples and 2.7% to 3.1% for 5-bar samples, indicating a good homogeneity of I_c over samples cut from a length of conductor of about 11 m for each group.

At 16 T, average J_c was 3230 and 1217 A/mm^2 for the 50- and 5-bar samples respectively, representing an increase by a factor 2.65 for the densified samples. This factor increased gradually at lower magnetic fields to 2.70 at 10 T. At 16 T, average engineering critical-current density J_e was 649 and 245 A/mm^2 for the 50- and 5-bar samples respectively. The factor of increase of J_c (and J_e) for the 50-bar over 5-bar samples was slightly higher than that for I_c (2.5, as shown in Fig. 3) because the wire diameter decreased from 1.0 to 0.97 mm due to the densification of Bi-2212 filaments.

To facilitate comparisons with data in literature more commonly reported at 1 µV/cm [1], we indicate that average J_c and J_e for our 50-bar samples at this criterion were 3668 and 737 A/mm^2 at 16 T, respectively (and 3751 and 754 A/mm^2 at 15 T, respectively). The J_c (and J_e) performance of this wire was very high but below the highest reported for Bi-2212 conductors [1].

The great performance increase of the 50-bar samples is due to the enhanced connectivity of Bi-2212 grains resulting from filament densification [2]. Effectively, scanning-electron-microscopy images in Fig. 4 indicate that pores had disappeared from a 50-bar sample but remained in a 5-bar sample [large pores are highlighted by red circles in Fig. 4(d)]. They also show the presence of large black spots and white regions inside some filaments. These are alkaline Earth cuprate (Sr, Ca)$_{14}$Cu$_{24}$O$_x$ (AEC-14:24), and Bi-2201 phase or

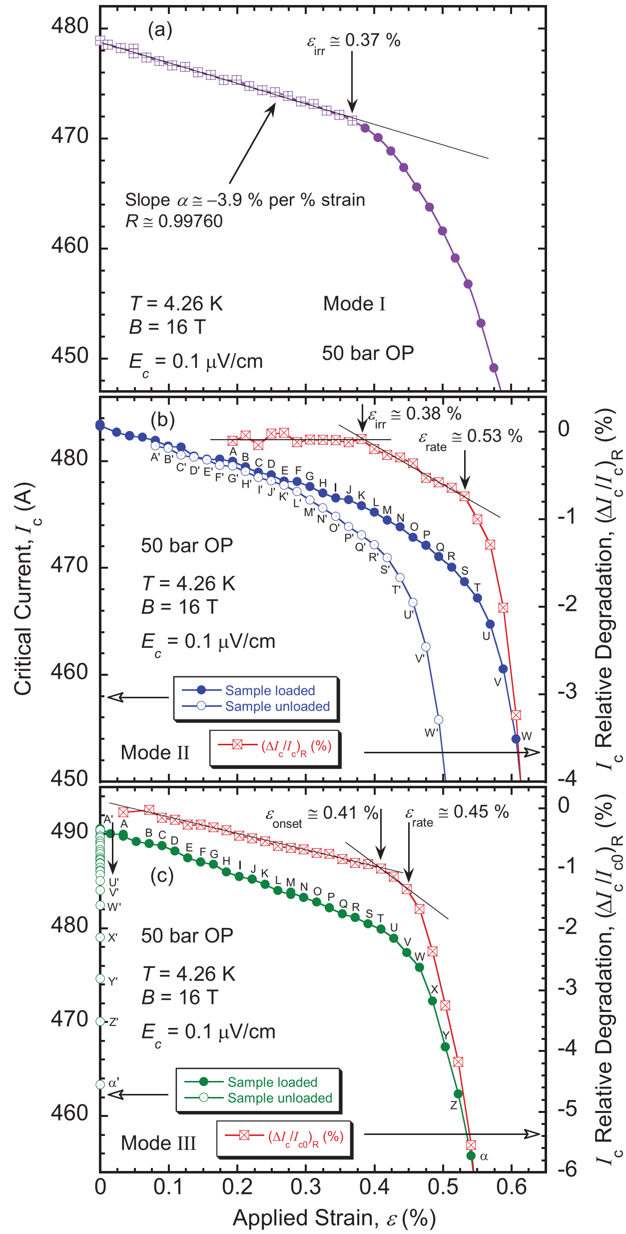

Fig. 5. Examples of $I_c(\varepsilon)$ results obtained on 50-bar Bi-2212 samples I-1, II-1, and III-1, measured in (a) the monotonic-loading mode (I), (b) the load/partial-unload mode (II), and (c) the load/full-unload mode (III), respectively, at 16 T, 4.26 K, and 0.1 µV/cm.

Ag, respectively. We note that Bi-2212 filaments had merged significantly, in both 5- and 50-bar samples.

B. Tensile Strain Effects on Densified and Nondensified Samples

1) Characteristic Strains: Examples of the results obtained in the three measurement modes on 50-bar samples I-1, II-1, and III-1 are displayed in Fig. 5 (also see [42]). An illustrative oral presentation is reported in [48].

For the monotonic-loading mode (I), in which reversibility of $I_c(\varepsilon)$ cannot be checked directly, we examined $I_c(\varepsilon)$ linearity and determined strain where it ceases as potentially being ε_{irr}—note

TABLE I
CHARACTERISTIC STRAINS AND RELATED PARAMETERS OBTAINED ON DENSIFIED BI-2212 SAMPLES MEASURED IN MODES I AND II AT $E_c = 0.1$ μV/CM

50 bar OP-HT		Slope α (% per % strain)	Coefficient R	ε_{irr} (%)	$(\Delta I_c/I_{c0})_T$ at ε_{irr} (%)	$\varepsilon_{2\%}$ (%)	ε_{rate} (%)	$(\Delta I_c/I_{c0})_T$ at ε_{rate} (%)	$\varepsilon_{5\%}$ (%)
Monotonic-Loading Mode (I)									
Sample I-1	Tap 1	–4.1	0.99846	0.39	–1.5	0.45	--	--	0.58
Δε = 0 %	Tap 2	–3.9	0.99760	0.37	–1.5	0.42	--	--	0.55
	Tap 3*	–3.9	0.99877	0.46	–1.4	0.53	--	--	0.60
Load/Partial-Unload Mode (II)									
Sample II-1	Tap 1	–4.0	0.99745	0.38	–1.6	0.44	0.53	–3.0	0.59
Δε = –0.11 %	Tap 2	–4.1	0.99753	0.42	–1.8	0.45	0.51	–2.6	0.59
	Tap 3	–4.2	0.99859	0.41	–1.7	0.44	0.49	–2.5	0.57
Sample II-2	Tap 1	–4.1	0.99696	0.42	–1.8	0.44	0.50	–2.6	0.59
Δε = –0.15 %	Tap 2	–4.1	0.99713	0.42	–1.8	0.44	0.50	–2.8	0.56
	Tap 3	–3.6	0.99458	0.46	–1.7	0.50	0.56	–2.7	0.62
	Average	–4.0	--	0.41	–1.7	0.46	0.52	–2.7	0.58
	s [a]	0.2	--	0.03	0.1	0.04	0.03	0.2	0.02

*See Appendix 1 of reference [42]
[a] s is the standard deviation.

that $I_c(\varepsilon)$ linear decrease for $\varepsilon \leq \varepsilon_{\rm irr}$ is correlated to T_c decrease with ε reported in [49]. Fig. 5(a) depicts such data and analysis for tap 2 of sample I-1. Data points for the linear fit are selected to maximize the correlation coefficient R. They are differentiated in Fig. 5(a) with square symbols for clarity. $I_c(\varepsilon)$ linearity alone is not necessarily a proof for $I_c(\varepsilon)$ reversibility unless the slope $\alpha = {\rm d}I_c/{\rm d}\varepsilon$ is small enough (typically $\leq$ –4% per % strain at 4 K) [42]. Steeper slope α may be indicative of an irreversible behavior.

Data obtained in the load/partial-unload mode (II) are shown in Fig. 5(b) for tap 1 of sample II-1, where the solid and empty circle symbols plotted on the left Y-axis represent $I_c(\varepsilon)$ when the sample is loaded and partially unloaded. They are indicated by a pair of unprimed and primed letters, respectively. The unloading strain step $\Delta\varepsilon$ was –0.11% for this sample. The I_c relative degradation $(\Delta I_c/I_c)_{\rm R}$ is plotted on the right Y-axis by use of rectangular symbols. $(\Delta I_c/I_c)_R$ represents I_c drop at a given (partially) unloaded strain point relative to I_c at the loaded strain point that had the same applied strain [for example points T' and N in Fig. 5(b)]. In each case, $(\Delta I_c/I_c)_R$ was assigned the strain value corresponding to the point from where strain was partially unloaded (for example, strain of point T in the previous example). $(\Delta I_c/I_c)_R$ was essentially zero at first, indicating reversibility of $I_c(\varepsilon)$ up to $\varepsilon_{\rm irr}$ where $(\Delta I_c/I_c)_R$ started decreasing. This decrease was gradual over a certain strain range and then became more significant starting at $\varepsilon_{\rm rate}$. This characteristic strain $\varepsilon_{\rm rate}$, introduced in [42], marks the first change of the I_c degradation rate in the irreversible domain. $\varepsilon_{\rm rate}$ may not be obvious from $I_c(\varepsilon)$ curve, but $(\Delta I_c/I_c)_R$ analysis reveals it. The total degradation $(\Delta I_c/I_{c0})_T$—with respect to the first value I_{c0} at zero strain—at $\varepsilon_{\rm rate}$ is –3 % in this case. It puts $\varepsilon_{\rm rate}$ between the characteristic strains $\varepsilon_{2\%}$ and $\varepsilon_{5\%}$ (see Fig. 1). Note also that $\varepsilon_{2\%}$ is higher than $\varepsilon_{\rm irr}$ where $(\Delta I_c/I_{c0})_T$ is –1.6 %.

Modes I and II produced very consistent results for the 50-bar samples throughout the entire strain range measured. Numerical data for these samples are summarized in Table I. Average characteristic-strain values for samples I-1, II-1 and II-2 were $\varepsilon_{\rm irr} = (0.41 \pm 0.03)$ %, $\varepsilon_{2\%} = (0.46 \pm 0.04)$ %, $\varepsilon_{\rm rate} = (0.52 \pm 0.03)$ %, and $\varepsilon_{5\%} = (0.58 \pm 0.02)$ %. The slope $\alpha = (–4.0 \pm 0.2)$ % per % strain.

For the load/full-unload mode (III), data are shown in Fig. 5(c) for tap 3 of sample III-1. The solid and empty circle symbols plotted on the left Y-axis (also indicated by a pair of unprimed and primed letters, respectively) represent $I_c(\varepsilon)$ when the sample is loaded and fully unloaded to zero applied strain (i.e., zero strain of the spring device, not necessarily of the sample that may have yielded under the prior loading strain, in which case the sample would be forced into longitudinal compression when the spring is brought back to zero applied strain). The unloading strain step $\Delta\varepsilon$ is variable throughout the measurements. The I_c relative degradation $(\Delta I_c/I_{c0})_R$ for each unloaded data point relative to I_{c0} is plotted on the right Y-axis by use of a rectangular symbol and assigned the strain value that corresponds to the point from where strain was fully unloaded (as explained above and in [42] and [48]). Note that $(\Delta I_c/I_{c0})_R$ is not the same as the total degradation $(\Delta I_c/I_{c0})_T$. $(\Delta I_c/I_{c0})_R$ is, for example, I_c drop of point Z′ with respect to I_{c0}, whereas $(\Delta I_c/I_{c0})_T$ is the I_c drop of point Z with respect to I_{c0}. Apart from the first two points, $(\Delta I_c/I_{c0})_R$ was not flat, indicating an irreversible

TABLE II
CHARACTERISTIC STRAINS AND RELATED PARAMETERS OBTAINED ON A DENSIFIED BI-2212 SAMPLE MEASURED IN MODE III AT $E_c = 0.1$ μV/CM

Load/Full-Unload Mode (III)										
50 bar OP-HT		Slope α (% per % strain)	Coefficient R	ε_{onset} (%)	$(\Delta I_c/I_{c0})_T$ at ε_{onset} (%)	$\varepsilon_{2\%}$ (%)	ε_{rate} (%)	$(\Delta I_c/I_{c0})_T$ at ε_{rate} (%)	$\varepsilon_{5\%}$ (%)
Sample III-1 Δε variable	Tap 1	–5.5	0.99817	0.35	–1.9	0.36	0.45	–2.8	0.53
	Tap 2	–5.5	0.99742	0.33	–1.8	0.36	0.42	–2.7	0.50
	Tap 3	–5.3	0.99853	0.41	–2.2	0.38	0.45	–2.7	0.51
	Average	–5.4	--	0.36	–2.0	0.37	0.44	–2.7	0.51
	s [a]	0.1	--	0.04	0.2	0.01	0.02	0.1	0.02

[a] s is the standard deviation.

TABLE III
CHARACTERISTIC STRAINS AND RELATED PARAMETERS OBTAINED ON NONDENSIFIED BI-2212 SAMPLES MEASURED IN MODES I AND II AT $E_c = 0.1$ μV/CM

Monotonic-Loading Mode (I)									
5 bar OP-HT		Slope α (% per % strain)	Coefficient R	ε_{irr} (%)	$(\Delta I_c/I_{c0})_T$ at ε_{irr} (%)	$\varepsilon_{2\%}$ (%)	ε_{rate} (%)	$(\Delta I_c/I_{c0})_T$ at ε_{rate} (%)	$\varepsilon_{5\%}$ (%)
Sample I-2 Δε = 0 %	Tap 1	–3.2	0.99407	0.27	–0.9	0.35	--	--	0.42
	Tap 2*	–3.3	0.99758	0.47	–0.8	0.53	--	--	0.56
	Tap 3	–2.8	0.99530	0.38	–1.1	0.42	--	--	0.47
Sample I-3 Δε = 0 %	Tap 1	–3.6	0.99619	0.24	–0.9	0.34	--	--	0.41
	Tap 2	–3.6	0.99887	0.30	–1.1	0.38	--	--	0.46
	Tap 3	–2.9	0.99759	0.36	–1.0	0.41	--	--	0.47
Load/Partial-Unload Mode (II)									
5 bar OP-HT		Slope α (% per % strain)	Coefficient R	ε_{irr} (%)	$(\Delta I_c/I_{c0})_T$ at ε_{irr} (%)	$\varepsilon_{2\%}$ (%)	ε_{rate} (%)	$(\Delta I_c/I_{c0})_T$ at ε_{rate} (%)	$\varepsilon_{5\%}$ (%)
Sample II-3 Δε = –0.11 %	Tap 1	–3.3	0.99702	0.27	–0.9	0.35	0.31	–1.2	0.42
	Tap 2	–3.1	0.99620	0.27	–0.9	0.38	0.35	–1.4	0.46
	Tap 3	–3.1	0.99701	0.24	–0.8	0.34	0.29	–1.2	0.41
	Average	–3.2	--	0.31	–0.9	0.39	0.32	–1.3	0.45
	s [a]	0.3	--	0.08	0.1	0.1	0.03	0.1	0.05

*See Appendix 1 of reference [42]
[a] s is the standard deviation.

$I_c(\varepsilon)$ behavior in this mode. $(\Delta I_c/I_{c0})_R$ decreased linearly and very progressively up to $\varepsilon_{\text{onset}}$, then at slightly higher rate up to $\varepsilon_{\text{rate}}$ where the degradation rate started to become more noticeable. Characteristic strains are summarized in Table II for mode III. Their average values were $\varepsilon_{\text{onset}} = (0.36 \pm 0.04)\%$, $\varepsilon_{2\%} = (0.37 \pm 0.01)\%$, $\varepsilon_{\text{rate}} = (0.44 \pm 0.02)\%$, and $\varepsilon_{5\%} = (0.51 \pm 0.02)\%$. The slope $\alpha = (–5.4 \pm 0.1)\%$ per % strain was steeper by 35% compared to that in modes I and II (see Tables I and II). As explained above, this is indicative of irreversibility, originating from the possibility that the sample, upon full unloading in mode III, may be under longitudinal compression (due to sample yielding prior to unloading) rather than being caused by tensile strain directly.

Examples of results obtained on 5-bar samples I-3, II-3, and III-2 (taps 3, 2, and 1 respectively) are depicted in Fig. 6 and Tables III and IV. For modes I and II, average characteristic-strain values were $\varepsilon_{\text{irr}} = (0.31 \pm 0.08)\%$, $\varepsilon_{\text{rate}} = (0.32 \pm 0.03)\%$, $\varepsilon_{2\%} = (0.39 \pm 0.1)\%$, and $\varepsilon_{5\%} = (0.45 \pm 0.05)\%$. It is clear that these characteristic strains were lower than those for the 50-bar samples and were more scattered (standard deviation s was higher). Also note that $\varepsilon_{\text{rate}} < \varepsilon_{2\%}$. The slope $\alpha = (–3.2 \pm 0.3)\%$ per % strain was quite consistent with values reported for older, nondensified, wires [31]. It was about 20% smaller (in absolute value) than that of densified samples. Strain effects remain very weak in the moderate strain range even for densified samples, nevertheless.

For mode III, average values were $\varepsilon_{\text{onset}} = (0.36 \pm 0.06)\%$, $\varepsilon_{2\%} = (0.40 \pm 0.07)\%$, $\varepsilon_{\text{rate}} = (0.42 \pm 0.08)\%$, and $\varepsilon_{5\%} = (0.49 \pm 0.08)\%$. In this case, characteristic strains were similar to those of the 50-bar sample III-1. However, they were more scattered. The slope $\alpha = (–4.4 \pm 0.4)\%$ per % strain was also steeper by 36% compared to that in modes I and II (see Tables III and IV).

TABLE IV
CHARACTERISTIC STRAINS AND RELATED PARAMETERS OBTAINED ON A NONDENSIFIED BI-2212 SAMPLE MEASURED IN MODE III AT $E_c = 0.1$ μV/CM

Load/Full-Unload Mode (III)									
5 bar OP-HT		Slope α (% per % strain)	Coefficient R	ε_{onset} (%)	$(\Delta I_c/I_{c0})_T$ at ε_{onset} (%)	$\varepsilon_{2\%}$ (%)	ε_{rate} (%)	$(\Delta I_c/I_{c0})_T$ at ε_{rate} (%)	$\varepsilon_{5\%}$ (%)
Sample III-2	Tap 1	–4.6	0.99605	0.40	–1.9	0.41	0.46	–2.5	0.51
Δε variable	Tap 2	–4.6	0.99566	0.29	–1.3	0.33	0.33	–1.9	0.40
	Tap 3	–3.9	0.99893	0.40	–1.6	0.46	0.48	–2.2	0.55
	Average	–4.4	--	0.36	–1.6	0.40	0.42	–2.2	0.49
	s [a]	0.4	--	0.06	0.3	0.07	0.08	0.3	0.08

[a] s is the standard deviation.

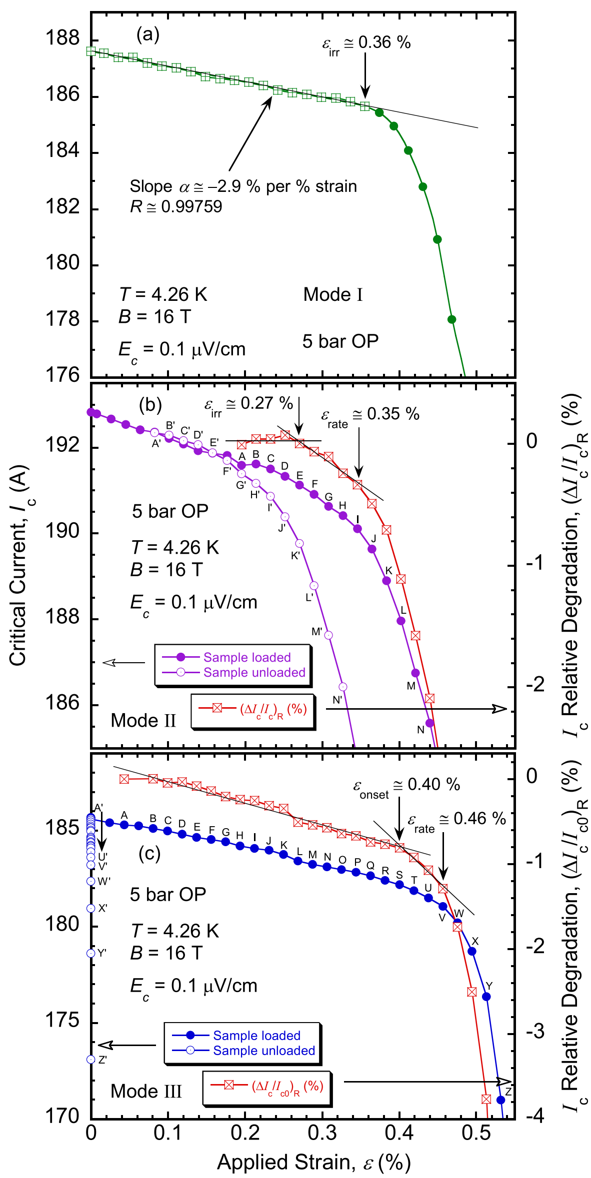

Fig. 6. Examples of $I_c(\varepsilon)$ results obtained on 5-bar Bi-2212 samples I-3, II-3, and III-2, measured in (a) the monotonic-loading mode (I), (b) the load/partial-unload mode (II), and (c) the load/full-unload mode (III), respectively, at 16 T, 4.26 K, and 0.1 μV/cm.

These results show that nondensified samples display a nonuniform response to strain. In contrast, densified samples have a noticeably more uniform response and higher values for the characteristic strains for the vast majority of cases. In the following, we will show direct comparisons between nondensified and densified samples, mode by mode, to highlight these differences.

2) Densification and Strain-Response Uniformity: Direct comparisons of the results obtained for the 50- and 5-bar samples are displayed in Figs. 7 –9 where both raw and normalized I_c versus ε data were plotted for modes I, II, and III, respectively, for the whole range of strain applied to these samples. These plots quite convincingly show that densification of Bi-2212 resulted in a rather uniform response of the conductor to strain, for all three measurement modes. In contrast, nondensified samples have an inhomogeneous response, whereas few segments of nondensified samples matched characteristic strains of densified samples, other segments showed degraded and disparate strain properties (as in Fig. 9). Figs. 7–9 illustrate a clear improvement of the overall strain properties of densified samples. This is a very positive consequence of Bi-2212 densification, additional to the large increase of I_c it generates.

C. Compressive Strain Effects on Densified and Nondensified Samples

Effects on I_c of longitudinal compressive strain were investigated down to –1% strain in mode I on 50- and 5-bar samples I-c1 and I-c2, respectively. Results are depicted in Fig. 10 for raw and normalized I_c versus ε data. The decrease of I_c with ε was progressive at moderate compressive strain and quite similar down to $\varepsilon \approx -0.28\%$. Beyond this strain value, sensitivity of the 50-bar samples to longitudinal compression became significantly higher, leading to a total degradation of I_c at $\varepsilon \approx -1\%$ of about 40% versus 25% for 5-bar samples [see Fig. 10(b)]. Before the cross-over strain of –0.28%, densified samples were marginally less sensitive, as shown in Fig. 11.

IV. DISCUSSION

Instead of pinpointing a strain limit for designing Bi-2212 magnets, we provided four characteristic strains marking the

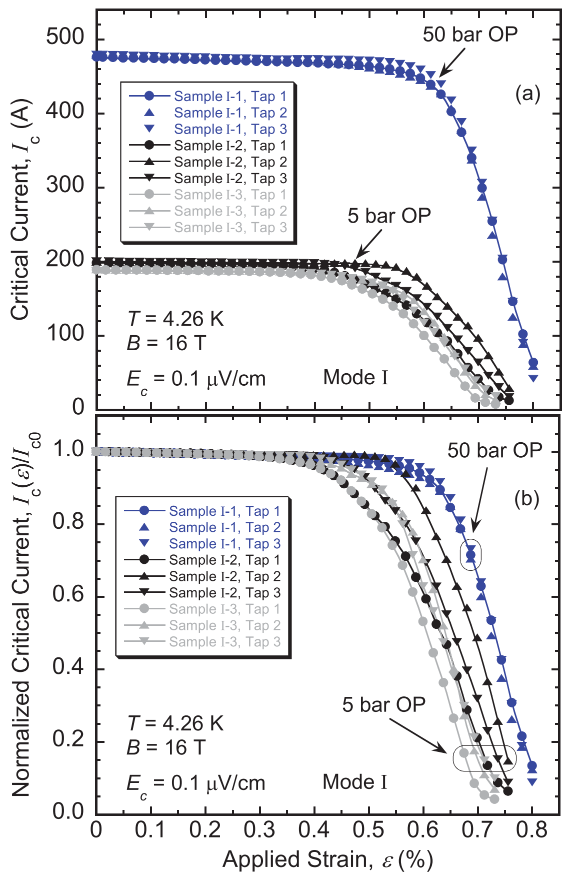

Fig. 7. Comparison of (a) raw and (b) normalized I_c versus tensile strain data obtained on densified (50-bar OP) and nondensified (5-bar OP) samples in the monotonic-loading mode (I) at 16 T and 4.26 K, and 0.1 µV/cm. Densification of Bi-2212 resulted in a significantly more uniform response of the conductor to strain and an increase of the characteristic strains.

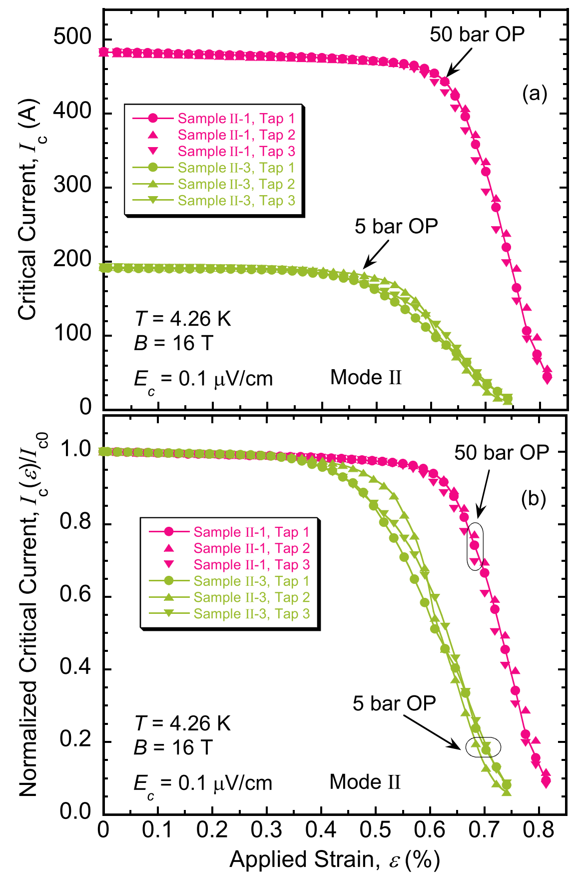

Fig. 8. Comparison of (a) raw and (b) normalized I_c versus tensile strain data obtained on densified (50-bar OP) and nondensified (5-bar OP) samples in the load/partial-unload mode (II) at 16 T, 4.26 K, and 0.1 µV/cm. Densification of Bi-2212 resulted in a significantly more uniform response of the conductor to strain and an increase of the characteristic strains.

transition of $I_c(\varepsilon)$ from weak to steeper dependences, for each of the samples studied herein. Debating what characteristic strain gives the proper measure of the conductor's strain limit for designing magnets may require additional experiments, such as fatigue cycling [50].

Average value of $\varepsilon_{\rm irr}$ increased from 0.31% for nondensified samples to 0.41% for densified samples (measured in mode I and II). Elimination of porosity in densified samples is plausibly behind the improvement of $\varepsilon_{\rm irr}$ (and the other characteristic strains in tension) and the more uniform response of the densified conductor to strain. The more homogenous microstructure of densified samples, which contrasts with stochastic distributions of pores along the length in nondensified specimen, most likely improves the conductor's strain properties and brings them into uniformity. This is a significant result that provides answers concerning densification effects on the conductor's strain properties. However, it is not yet known if these effects reproduce in conductors made with different powders (having different grain-size distribution, for example) or with different designs (such as filament spacing, for example).

Beyond $\varepsilon_{\rm irr}$, from 0.4% to about 0.6% strain, irreversible degradation increased very progressively. Irregularities in filament shape and their degree of merging may have some influence on this behavior. If these features of the conductor can be controlled [43], it would provide opportunities for examining this supposition.

It would be useful to establish at what strain cracks start forming in Bi-2212. Bjoerstad et al. [37] reported that stress versus strain curve at 77 K reaches a plateau at a strain of 0.6%, which value coincided with $\varepsilon_{5\%}$. The 5% degradation in their work is likely related to $(\Delta I_c/I_c)_R$, not $(\Delta I_c/I_{c0})_T$. In fact, $(\Delta I_c/I_{c0})_T$ was close to 20% at 0.6% strain [37] because the slope α becomes significantly steeper at temperatures >>4.2 K [49]. Bjoerstad et al. [37] interpreted the plateauing of the stress versus strain curve as being due to filament fracturing, given that filaments can no longer carry higher loads at that point. It is plausible that fracturing of most filaments will saturate the stress level that is then carried mostly by Ag and Ag-Mg matrix, which deform plastically at strains significantly lower than 0.6%. However, the beginning of the stress versus strain plateau may not necessarily indicate the *onset* of filament fracturing. This onset is likely located at a lower strain value, where irreversibility starts and $I_c(\varepsilon)$ deviates from linearity, i.e., at $\varepsilon_{\rm irr}$, not higher.

Comparison of the results in tension for densified samples showed that modes I and II are equivalent (for $\Delta\varepsilon$ at least up to

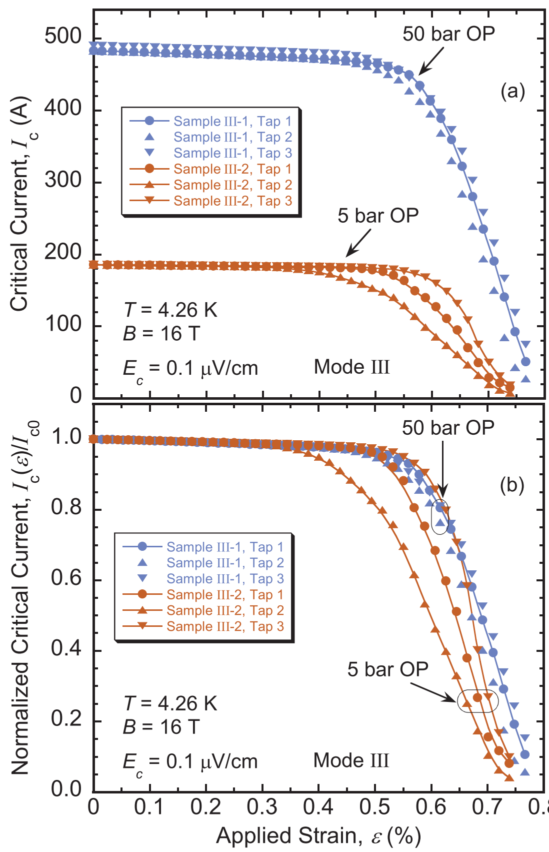

Fig. 9. Comparison of (a) raw and (b) normalized I_c versus tensile strain data obtained on densified (50-bar OP) and nondensified (5-bar OP) samples in the load/full-unload mode (III) at 16 T, 4.26 K, and 0.1 μV/cm. Densification of Bi-2212 resulted in a significantly more uniform response of the conductor to strain. Even though average values of the characteristic strains did not change much in this case, the densified sample still showed a better resilience to strain.

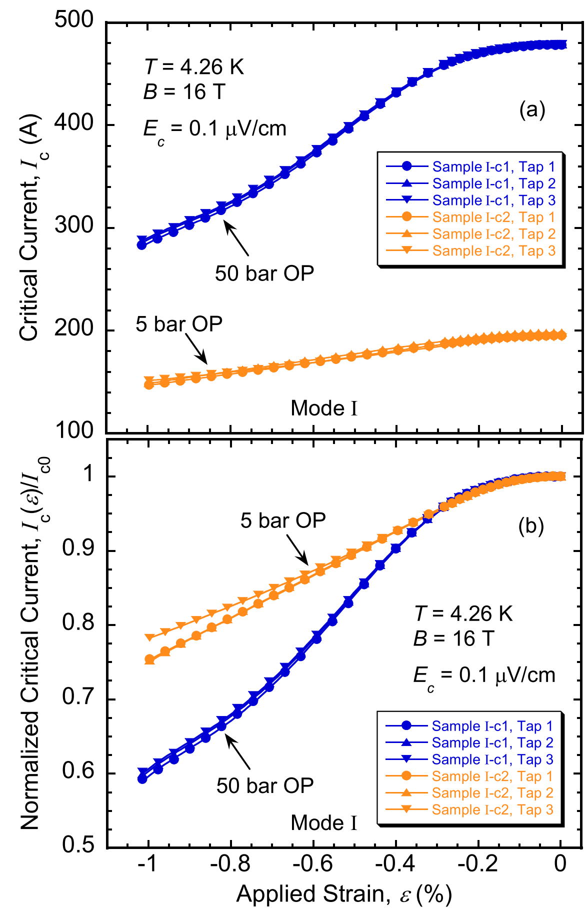

Fig. 10. Comparison of (a) raw and (b) normalized I_c versus compressive strain data obtained on densified (50-bar OP) and nondensified (5-bar OP) samples in the monotonic-loading mode (I) at 16 T, 4.26 K, and 0.1 μV/cm. Sensitivity of the densified sample to compressive strain increased significantly for strains beyond −0.28%.

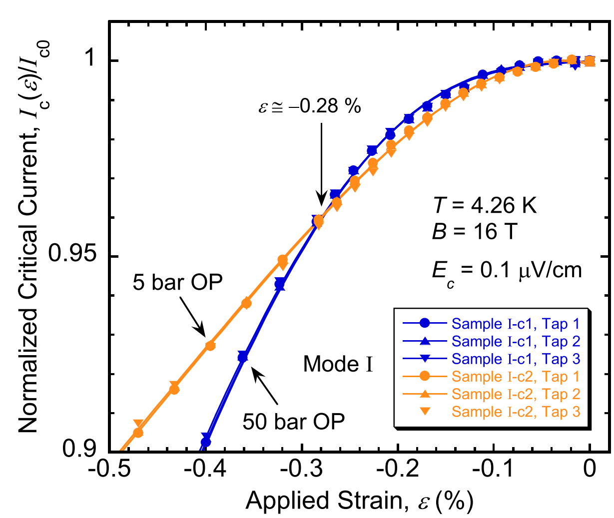

Fig. 11. Comparison of normalized I_c versus compressive strain data obtained on densified (50-bar OP) and nondensified (5-bar OP) samples in the monotonic-loading mode (I) at 16 T, 4.26 K, and 0.1 μV/cm, showing in more detail data of Fig. 10(b). Sensitivity of the densified sample to compressive strain increased significantly for strains beyond –0.28%, but was slightly less for strains before −0.28%.

−0.15 %), whereas mode III tends to shift $I_c(\varepsilon)$ curve to lower strain values [42]. This is consistent with our expectations that mode III would be more severe. However, this trend did not hold for nondensified samples where data were scattered in a way that did not correlate with measurement-mode severity (see Figs. 7–9). We believe that effects of these measurement modes in nondensified samples are masked by sample inhomogeneity.

In the modified descriptive strain model (MDSM), Cheggour et al. speculated that the linear behavior of $I_c(\varepsilon)$ in tension may extend into longitudinal compression if Bi-2212 filaments are densified and Ag matrix between Bi-2212 filaments is replaced by a stronger material to prevent buckling of Bi-2212 grains [31]. This hypothesis was based on the Bi-2212 buckling being the main reason for I_c degradation in longitudinal compression. If buckling were to be prevented such that longitudinal compression only produces elastic deformations of the Bi-2212 crystal lattice, a priori, there should be no reason for the $I_c(\varepsilon)$ linear dependence in tension not to continue into compression. So far, no alternative material to Ag has been identified and so we cannot really verify this MDSM hypothesis. Nevertheless, we notice a plateau of $I_c(\varepsilon)$ for small compressive strain values down to −0.05% (see Fig. 11). This was not observed in the older

Bi-2212 wires studied in [31]. An extension of the $I_c(\varepsilon)$ linear behavior into the compressive strain regime may be possible but could be limited to a very small strain range if buckling is difficult to prevent.

The more pronounced sensitivity to high compressive strain in densified samples is surprising though anticipated by Godeke et al. [35]. Possibly, in compression, strain-induced defects propagate more easily in densified than in porous Bi-2212 filaments, where pores may block these defects from expanding and thus limit I_c degradation. Just as filament densification provides bigger cross-sections for transporting supercurrents through the wire filaments and results in significantly higher I_c values (see Fig. 3), it also provides material continuums that probably allow compression-induced defects to propagate more easily for strain beyond -0.28% (in the case of the samples studied herein). In contrast, pores in nondensified samples likely arrest these defects and thus keep damage relatively more localized. In this understanding, we note that pores are considered initiators of cracks in tension and arrestors of defects (buckling and other) formed in compression. More studies may be needed to elucidate these seemingly opposite effects of porosity.

The difference in sensitivity to longitudinal compressive strain is useful academically to understand the mechanisms of failure in Bi-2212 conductors but should have no significant repercussions for applications, nonetheless. In effect, despite their higher sensitivity at large compression, I_c values of densified samples remain at least twice as high as those of nondensified samples [see Fig. 10(a)]. Thus, densification of Bi-2212 conductors is extremely beneficial under all longitudinal-strain situations for the samples examined herein.

V. Conclusion

A detailed study has been made on a very high J_c Bi-2212 conductor, made with fine Engi-Mat powder, under two OP-HT conditions that enabled us to compare properties with and without residual porosity. We found that behavior was much more uniform in longitudinal tension for fully densified 50 bar OP-HT samples compared to 5 bar OP-HT samples where residual porosity was present. The characteristic strains, which we used to describe the transition of $I_c(\varepsilon)$ from weak to steeper dependences in tension, also increased for densified samples, indicating that residual pores do degrade the tensile strain (and J_c) performance. These results do demonstrate that densification improved the strain resilience of the Bi-2212 conductor investigated.

First irreversible $I_c(\varepsilon)$ degradation of densified samples occurred around 0.4% strain, the degradation then increased progressively over the strain range of 0.4%–0.6%. Local stress concentrations in the highly irregular Bi-2212 filament structure and the highly merged filaments might control damage. If filament irregularities and merging could be controlled by changing the wire design and OP-HT parameters, this hypothesis would be worth exploring. Also, the relevance of the progressive damage within the 0.4%–0.6% strain range to magnet-design practices should be evaluated.

The sensitivity of densified samples to longitudinal compressive strain increased significantly in comparison to that of nondensified samples for strains beyond –0.28%. Plausibly, densification provides a continuum of Bi-2212 material through which defects generated under longitudinal compression can propagate over longer lengths, and thus generate more degradation, as compared to nondensified samples where pores probably act as arrestors of these defects and limit their progression. Nevertheless, densification effects remain extremely beneficial despite the increase in strain sensitivity under compression.

References

[1] J. Jiang et al., "High-performance Bi-2212 round wires made with recent powders," *IEEE Trans. Appl. Supercond.*, vol. 29, no. 5, Aug. 2019, Art. no. 6400405, doi: 10.1109/TASC.2019.2895197.

[2] D. C. Larbalestier, "Isotropic round-wire multifilament cuprate superconductor for generation of magnetic fields above 30 T," *Nature Mater.*, vol. 13, pp. 375–381, 2014, doi: 10.1038/NMAT3887.

[3] M. R. Matras, E. E. Hellstrom, U. P. Trociewitz, J. Jiang, and D. C. Larbalestier, "Densified superconductor materials and methods," Patent No. US010450641B2, Oct. 22, 2019.

[4] M. R. Matras, J. Jiang, U. P. Trociewitz, D. C. Larbalestier, and E. E. Hellstrom, "Process to densify $Bi_2Sr_2CaCu_2O_X$ round wire with overpressure before coil winding and final overpressure heat treatment," *Supercond. Sci. Technol.*, vol. 33, 2020, Art. no. 025010, doi: 10.1088/1361-6668/ab5ad6.

[5] Y. Huang, H. Miao, S. Hong, and J. A. Parrell, "Bi-2212 round wire development for high field applications," *IEEE Trans. Appl. Supercond.*, vol. 24, no. 3, Jun. 2014, Art. no. 6400205, doi: 10.1109/TASC.2013.2281063.

[6] F. Kametani et al., "Bubble formation within filaments of melt-processed Bi2212 wires and its strongly negative effect on the critical current density," *Supercond. Sci. Technol.*, vol. 24, 2011, Art. no. 075009, doi: 10.1088/0953-2048/24/7/075009.

[7] J. Jiang et al., "Doubled critical current density in Bi-2212 round wires by reduction of the residual bubble density," *Supercond. Sci. Technol.*, vol. 24, 2011, Art. no. 082001, doi: 10.1088/0953-2048/24/8/082001.

[8] C. Scheuerlein et al., "Void and phase evolution during the processing of Bi-2212 superconducting wires monitored by combined fast synchrotron micro-tomography and X-ray diffraction," *Supercond. Sci. Technol.*, vol. 24, 2011, Art. no. 115004, doi: 10.1088/0953-2048/24/11/115004.

[9] A. T. Hunt and H. G. Hornis, "Chemical vapor deposition and powder formation using thermal spray with near supercritical and supercritical fluid solutions," Patent No. US006132653A, Oct. 2000.

[10] S. Sengupta et al., "Synthesis of bismuth-strontium-calcium-copper oxide powders for silver composite wires with uniform micron sized filaments," *IEEE Trans. Appl. Supercond.*, vol. 9, no. 2, pp. 2601–2604, Jun. 1999, doi: 10.1109/77.785019.

[11] T. Shen and L. G. Fajardo, "Superconducting accelerator magnets based on high-temperature superconducting Bi-2212 round wires," *Instruments*, vol. 4, 2020, Art. no. 17, doi: 10.3390/instruments4020017.

[12] H. Bai et al., "The 40 T superconducting magnet project at the national high magnetic field laboratory," *IEEE Trans. Appl. Supercond.*, vol. 30, no. 4, Jun. 2020, Art. no. 4300405, doi: 10.1109/TASC.2020.2969642.

[13] L. Garcia Fajardo et al., "Fabrication of Bi-2212 canted-cosine-theta dipole prototypes," *IEEE Trans. Appl. Supercond.*, vol. 29, no. 5, Aug. 2019, Art. no. 4002005, doi: 10.1109/TASC.2019.2896725.

[14] T. Shen et al., "Stable, predictable and training-free operation of superconducting Bi-2212 Rutherford cable racetrack coils at the wire current density of 1000 A/mm^2," *Sci. Rep.*, vol. 9, 2019, Art. no. 10170, doi: 10.1038/s41598-019-46629-3.

[15] H. Maeda and Y. Yanagisawa, "Future prospects for NMR magnets: A perspective," *J. Magn. Reson.*, vol. 306, pp. 80–85, 2019, doi: 10.1016/j.jmr.2019.07.011.

[16] D. Uglietti, "A review of commercial high temperature superconducting materials for large magnets: From wires and tapes to cables and conductors," *Supercond. Sci. Technol.*, vol. 32, 2019, Art. no. 053001, doi: 10.1088/1361-6668/ab06a2.

[17] P. Chen et al., "Experimental study of potential heat treatment issues of large Bi-2212 coils," *IEEE Trans. Appl. Supercond.*, vol. 27, no. 4, Jun. 2017, Art. no. 4601405, doi: 10.1109/TASC.2017.2652849.

[18] A. Godeke et al., "Wind-and-react Bi-2212 coil development for accelerator magnets," *Supercond. Sci. Technol.*, vol. 23, 2010, Art. no. 034022, doi: 10.1088/0953-2048/23/3/034022.

[19] H. W. Weijers et al., "High field magnets with HTS conductors," *IEEE Trans. Appl. Supercond.*, vol. 20, no. 3, pp. 576–582, Jun. 2010, doi: 10.1109/TASC.2010.2043080.

[20] H. W. Weijers, U. P. Trociewitz, K. Marken, M. Meinesz, H. Miao, and J. Schwartz, "The generation of 25.05 T using a 5.11 T $Bi_2Sr_2CaCu_2O_x$ superconducting insert magnet," *Supercond. Sci. Technol.*, vol. 17, pp. 636–644, 2004, doi: 10.1088/0953-2048/17/4/012.

[21] H. W. Weijers et al., "Development of a 5 T HTS insert magnet as part of 25 T class magnets," *IEEE Trans. Appl. Supercond.*, vol. 13, no. 2, pp. 1396–1399, Jun. 2003, doi: 10.1109/TASC.2003.812677.

[22] Z.-H. Mao et al., "Axial tensile stress–strain characterization of Bi-2212 round wire with different heat treatments," *IEEE Trans. Appl. Supercond.*, vol. 27, no. 6, Sep. 2017, Art. no. 6400405, doi: 10.1109/TASC.2017.2721967.

[23] M. Brown et al., "Tensile properties and critical current strain limits of reinforced Bi-2212 conductors for high field magnets," *IOP Conf. Ser., Mater. Sci. Eng.*, vol. 279, 2017, Art. no. 012022, doi: 10.1088/1757-899X/279/1/012022.

[24] A. Kajbafvala et al., "Dispersion-strengthened silver alumina for sheathing $Bi_2Sr_2CaCu_2O_{8+x}$ multifilamentary wire," *IEEE Trans. Appl. Supercond.*, vol. 22, no. 1, Feb. 2012, Art. no. 8400210, doi: 10.1109/TASC.2011.2179296.

[25] X. F. Lu et al., "Electromechanical characterization of Bi-2212 strands," *IEEE Trans. Appl. Supercond.*, vol. 21, no. 3, pp. 3086–3089, Jun. 2011, doi: 10.1109/TASC.2010.2084061.

[26] E. S. Bosque, Y. Kim, U. P. Trociewitz, C. L. English, and D. C. Larbalestier, "System and method to manage high stresses in Bi-2212 wire wound compact superconducting magnets," Patent No. US20190392989A1, Dec. 2019.

[27] P. McIntyre, J. Breitschopf, T. E. Brown, D. Chavez, J. N. Kellams, and A. Sattarov, "SuperCIC: Enhanced winding current density for hybrid windings of Tokamaks," *IEEE Trans. Appl. Supercond.*, vol. 30, no. 4, Jun. 2020, Art. no. 4203407, doi: 10.1109/TASC.2020.2971195.

[28] P. M. McIntyre, J. Breitschopf, D. Chavez, J. N. Kellams, and A. Sattarov, "$>$16 T hybrid dipole for an LHC energy doubler," *IEEE Trans. Appl. Supercond.*, vol. 30, no. 4, Jun. 2020, Art. no. 4901906, doi: 10.1109/TASC.2020.2981301.

[29] T. Shen et al., "High strength kiloampere $Bi_2Sr_2CaCu_2O_x$ cables for high-field magnet applications," *Supercond. Sci. Technol.*, vol. 28, 2015, Art. no. 065002, doi: 10.1088/0953-2048/28/6/065002.

[30] W. D. Markiewicz, J. R. Miller, J. Schwartz, U. P. Trociewitz, and H. W. Weijers, "Perspective on a superconducting 30 T/1.3 GHz NMR spectrometer magnet," *IEEE Trans. Appl. Supercond.*, vol. 16, no. 2, pp. 1523–1526, Jun. 2006, doi: 10.1109/TASC.2005.869663.

[31] N. Cheggour, X. F. Lu, T. G. Holesinger, T. C. Stauffer, J. Jiang, and L. F. Goodrich, "Reversible effect of strain on transport critical current in $Bi_2Sr_2CaCu_2O_{8+x}$ superconducting wires: A modified descriptive strain model," *Supercond. Sci. Technol.*, vol. 25, 2012, Art. no. 015001, doi: 10.1088/0953-2048/25/1/015001.

[32] B. ten Haken, A. Godeke, H.-J. Schuver, and H. H. J. ten Kate, "Descriptive model for the critical current as a function of axial strain in Bi-2212/Ag wires," *IEEE Trans. Magn.*, vol. 32, no. 4, pp. 2720–2723, Jul. 1996, doi: 10.1109/20.511436.

[33] B. ten Haken, H. H. J. ten Kate, and J. Tenbrink, "Compressive and tensile axial strain reduced critical currents in Bi-2212 conductors," *IEEE Trans. Appl. Supercond.*, vol. 5, no. 2, pp. 1298–1301, Jun. 1995, doi: 10.1109/77.402800.

[34] B. ten Haken and H. H. J. ten Kate, "Lattice deformation in an axially strained BiSrCaCuO/Ag tape conductor investigated by X-ray diffraction," *Physica C*, vol. 270, no. 1-2, pp. 21–24, 1996, doi: 10.1016/0921-4534(96)00479-0.

[35] A. Godeke et al., "Critical current of dense Bi-2212 round wires as a function of axial strain," *Supercond. Sci. Technol.*, vol. 28, 2015, Art. no. 032001, doi: 10.1088/0953-2048/28/3/032001.

[36] K. Damborsky and J. Parrell, "Understanding and mitigating strain effects in Bi-2212/Ag conductors," *Supercond. Sci. Technol.*, vol. 28, 2015, Art. no. 050501, doi: 10.1088/0953-2048/28/5/050501.

[37] R. Bjoerstad et al., "Strain induced irreversible critical current degradation in highly dense Bi-2212 round wire," *Supercond. Sci. Technol.*, vol. 28, 2015, Art. no. 062002, doi: 10.1088/0953-2048/28/6/062002.

[38] U. P. Trociewitz, "Making strain effects inside Bi-2212/Ag conductors visible," *Supercond. Sci. Technol.*, vol. 28, 2015, Art. no. 070501, doi: 10.1088/0953-2048/28/7/070501.

[39] H. Chen et al., "Critical current under uniaxial strain on high-pressure heat treatment Bi-2212 round wire," *IEEE Trans. Appl. Supercond.*, vol. 30, no. 4, Jun. 2020, Art. no. 6400304, doi: 10.1109/TASC.2020.2975740.

[40] C. Dai et al., "Uniaxial strain induced critical current degradation of Ag-sheathed Bi-2212 round wire," *IEEE Trans. Appl. Supercond.*, vol. 28, no. 3, Apr. 2018, Art. no. 6400104, doi: 10.1109/TASC.2017.2787133.

[41] M. Sugano, K. Itoh, and T. Kiyoshi, "Strain dependence of critical current in Bi2212 W&R wires under magnetic field up to 30 T," *IEEE Trans. Appl. Supercond.*, vol. 16, no. 2, pp. 1039–1042, Jun. 2006, doi: 10.1109/TASC.2005.864323.

[42] N. Cheggour and E. L. Marks, "Protocols and methodologies for acquiring and analyzing critical-current versus longitudinal-strain data in $Bi_2Sr_2CaCu_2O_{8+x}$ wires," *Supercond. Sci. Technol.*, vol. 38, 2025, Art. no. 015012, doi: 10.1088/1361-6668/ad9ad9.

[43] J. Jianyi et al., "Effects of wire diameter and filament size on the processing window of Bi-2212 round wire," *IEEE Trans. Appl. Supercond.*, vol. 31, no. 5, Aug. 2021, Art. no. 6400206, doi: 10.1109/TASC.2021.3055475.

[44] C. R. Walters, I. M. Davidson, and G. E. Tuck, "Long sample high sensitivity critical current measurements under strain," *Cryogenics*, vol. 26, no. 7, pp. 406–412, 1986, doi: 10.1016/0011-2275(86)90085-8.

[45] N. Cheggour and D. P. Hampshire, "A probe for investigating the effects of temperature, strain, and magnetic field on transport critical currents in superconducting wires and tapes," *Rev. Sci. Instrum.*, vol. 71, pp. 4521–4530, 2000, doi: 10.1063/1.1324734.

[46] L. F. Goodrich, N. Cheggour, T. C. Stauffer, B. J. Filla, and X. F. Lu, "Kiloampere, variable-temperature, critical-current measurements of high-field superconductors," *J. Res. NIST*, vol. 118, pp. 301–352, 2013, doi: 10.6028/jres.118.015.

[47] A. Godeke et al., "A device to investigate the axial strain dependence of the critical current density in superconductors," *Rev. Sci. Instrum.*, vol. 75, pp. 5112–5118, 2004, doi: 10.1063/1.1819384.

[48] N. Cheggour and E. L. Marks, "On the need for protocols and standard procedures for studying $I_c(\varepsilon)$ in Bi-2212 wires," Oct. 2020. [Online]. Available: https://www.researchgate.net/publication/348480515_On_the_Need_for_Protocols_and_Standard_Procedures_for_Studying_Icstrain_in_Bi-2212_Wires, doi: 10.13140/RG.2.2.14787.2256.

[49] X. F. Lu et al., "Correlation between pressure dependence of critical temperature and the reversible strain effect on the critical current and pinning force in $Bi_2Sr_2CaCu_2O_{8+x}$ wires," *IEEE Trans. Appl. Supercond.*, vol. 22, no. 1, Feb. 2012, Art. no. 8400307, doi: 10.1109/TASC.2011.2174630.

[50] K. Osamura, S. Machiya, and G. Nishijima, "Reversible stress and strain limits of the critical current of practical REBCO and BSCCO wires," *Supercond. Sci. Technol.*, vol. 29, 2016, Art. no. 094003, doi: 10.1088/0953-2048/29/9/094003.

Najib Cheggour received the B.S. degree in physics from University Cadi Ayyad, Marrakech, Morocco, in 1986, and the M.S. and Ph.D. degrees in solid state physics from University Paul Sabatier, Toulouse, France, in 1987 and 1990, respectively.

He joined the University of Geneva, Geneva, Switzerland, as a Research Assistant, and then the University of Durham, Durham, U.K., as a Research Associate. He continued his research activities at the National Institute of Standards and technology (NIST), Gaithersburg, MD, USA, and University of Colorado at Boulder, Boulder, CO, USA, for more than 17 years. Since 2017, he has been a Research Faculty with the Applied Superconductivity Center, National High Magnetic Field Laboratory, Florida State University (ASC-NHMFL-FSU), Tallahassee, FL, USA. His research interests and expertise include the electromechanical properties of low- and high-temperature superconductors of interest to communities developing high-energy-physics particle accelerators, fusion-energy reactors, and medical imaging and radiation-therapy technologies; causalities between strain behavior, microstructural properties, and processing of superconductors; electric transport and flux-pinning properties; as well as metrology development for superconductor characterization.

Emsley L. Marks, biography not available at the time of publication.

Jianyi Jiang (Senior Member, IEEE), biography not available at the time of publication.

Ernesto Bosque, biography not available at the time of publication.

David C. Larbalestier (Fellow, IEEE), biography not available at the time of publication.